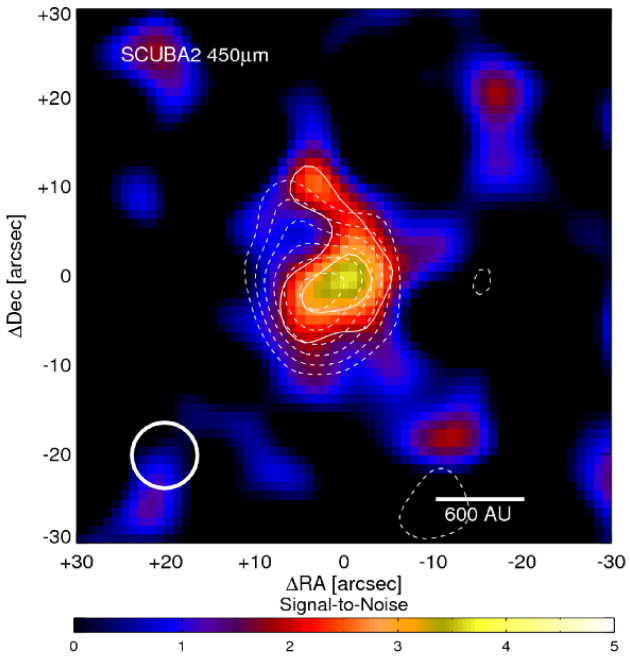

Figure 1. SCUBA-2 results for 49 Cet, on signal-to-noise ratio scales. The peak flux at 450 microns is is 74 ± 14 mJy/beam, and the integrated flux within a 40 arcsec diameter aperture is 125 ± 10 mJy. The dashed contours show the 850 μm SNR (peak = 8.3), overlaid on the 450 μm colour-scale. The integrated flux at 850 μm is 12.1 ± 2.0 mJy. The secondary peak adjacent to the north (top) side of the disc may be due to a background dusty galaxy. The stellar position coincides with the 450 μm flux-peak within typical pointing drifts ($\lesssim 2''$).

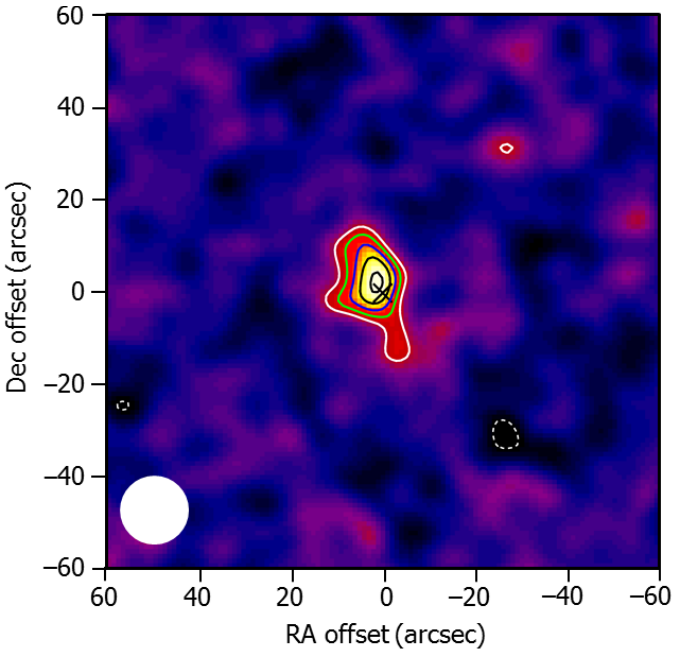

Figure 2. SCUBA-2 850 micron image for HD 21997, with contours at 3,4,5,6,7 sigma levels and a peak of 7.9 ± 1.1 mJy/beam. The integrated flux is 10.7 ± 1.5 mJy.

Here we consider debris-hosting A-stars within 125 pc (parallax ≥8 mas) that have been searched for CO. This distance limit helps to exclude stars outside the Local Bubble where interstellar CO may be a strong contaminant. We report the sixth detection of CO, around the approximately 30 Myr-old A0 star HD 32297. In this case, we successfully used the presence of weak CII emission (Donaldson et al. 2013) as a predictor for the presence of CO.

We have also followed CO detections for 49 Ceti and HD 21997 (Zuckerman et al. 1995; Moór et al. 2011) with dust continuum-imaging at 450 and 850 micron wavelength. These continuum data are part of the JCMT Legacy Project SONS (SCUBA-2 Survey of Nearby Stars), described by Panić et al. (2013). The gas-plus-dust systems are also tested here against model predictions that the short-lived CO component could be more spatially asymmetric than the dust.

2 OBSERVATIONS

The new data were obtained with the 15 m James Clerk Maxwell Telescope located on Mauna Kea, Hawaii. Observing procedures have been described by, for example, Panić et al. (2013, 2010). HD 21997 and 49 Cet were observed with the SCUBA-2 camera (Holland et al. 2013) in 2012-2015, in moderately dry conditions (225 GHz zenith opacities under 0.1). Images are shown with 1 arcsec pixels, and after smoothing with a 7-arcsec Gaussian, the effective beam diameters are 15.8 and 11.6 arcsec at 850 and 450 microns respectively. The continuum data reduction used the makemap task in the SMURF package (Jenness et al. 2011), plus high-pass filtering and zero-masking to remove residual low-frequency structure in the backgrounds.

The CO data for HD 32297 at 1.3 mm were taken as part of a poor weather backup programme in 2013 (225 GHz zenith opacities up to 0.3), using the RxA3 receiver to search for the J=2–1 transition. The spectral reduction used the makecube task in SMURF plus the SPLAT package for baselining and binning. A 200 km/s velocity range is shown around the stellar velocity in the heliocentric frame of 23.0 ± 0.3 km/s (Torres et al. 2006). After about 10 hours on sky, the JCMT J=2-1 data are about twice as sensitive as the corresponding spectrum of Zuckerman & Song (2012) from the IRAM 30m telescope.

3 RESULTS

3.1 Dust imaging

Figure 1 shows the SCUBA-2 data for 49 Cet. The disc is spatially resolved at 450 μm, at the expected orientation. For comparison, the position angle with Herschel at 70 μm (Roberge et al. 2013) is ≈ 105° (anti-clockwise from north), while CO lies at PA = 110 ± 10° (Hughes et al. 2008). The SExtractor tool for automatic object detection[1] was used here, indicating PA ≈ 120° for the 450 μm disc axis.

[1] The peak just to the north was assumed to be unrelated, and was blanked before fitting the disc.

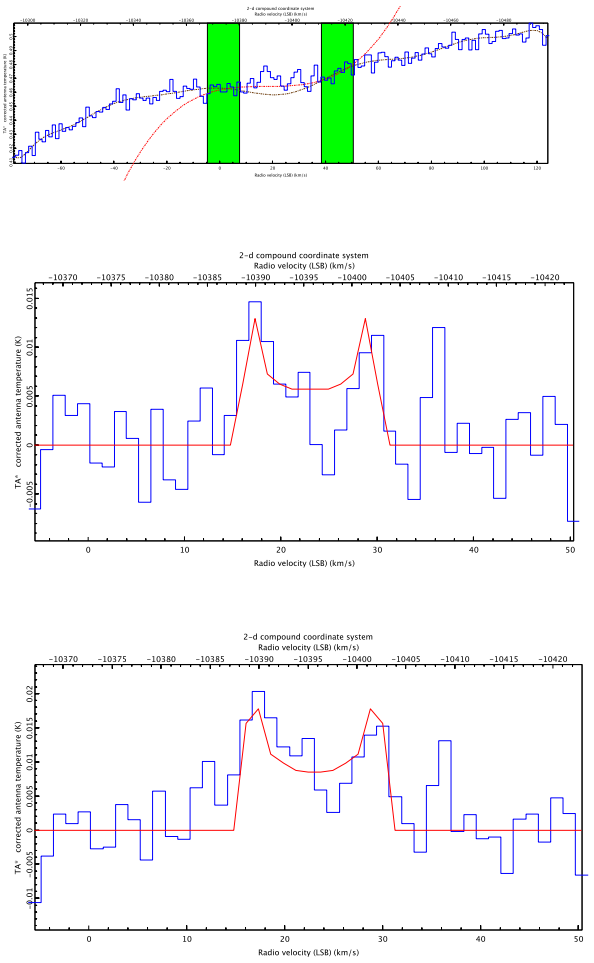

Figure 3. CO J=2-1 spectrum for HD 32297. Top: results from fitting the passband with wide and narrow (green-shaded) velocity ranges. Middle: spectrum after subtracting the 3rd-order polynomial shown in red in the top panel. Bottom: spectrum after subtracting the 14th-order polynomial shown in brown in the top panel. The two models shown by the red curves in the middle and bottom panels are for molecules on Keplerian orbits (see text).

At the half-power contour at 450 μm, the major:minor axis ratio is 1.52 from this fit. The long diameter is 17.7 arcsec and the minor axis is unresolved. This is consistent with the disc being seen close to edge-on – Lieman-Sifry & Hughes (2015) find an inclination of 79.6±0.4° from their ALMA 850 μm image. They also identify dust out to 286 ± 7 AU from the star, while our 450 μm image (after deconvolving the beam size in quadrature) gives a slightly larger outer radius, approximately 6.7 arcsec or 395 AU at 59 pc.

Figure 2 shows our 850 μm image of HD 21997. The structure appear asymmetric, with most of the flux centred in a peak slightly north of the star and only a 3-sigma counterpart to the south. In contrast, Moór et al. (2013) found a compact symmetric disc in their ALMA 886 μm image. However, they noted some extension along an axis at PA $\sim 20-25°$ in Herschel images at 70-100 μm. This agrees with the slightly east-of-north orientation seen in the SCUBA-2 image. To reconcile the submillimetre datasets, there could be significant flux beyond the half-power point of the ALMA primary beam (>9 arcsec, or 650 AU). The SCUBA-2 integrated flux in fact substantially exceeds the 2.7 ± 0.3 mJy in a 6-arcsec aperture from ALMA. Only 15 ALMA antennas were available to Moór et al., so some spatial scales may not have been fully sampled.

SCUBA-2 also simultaneously observed HD 21997 at 450 μm, and a tentative signal of 85 ± 25 mJy/beam was seen near the star. There is a similar peak about 15 arcsec SW of the star, but this appears to coincide with a faint part of the 850 μm background structure.

HD 32297 is not a SONS target, but has been imaged in dust emission at 1.3 mm by Manness et al. (2008), and was resolved at arcsec resolution. The disc was found to be extended and elliptical, with a strong asymmetry, in that the centroid is offset from the star with 4-sigma confidence.

3.2 CO spectroscopy

Figure 3 shows the CO spectrum towards HD 32297, reduced by two different methods to test for robustness. The entire passband was first fitted with a high-order polynomial, in order to fully use the information present, and excluding only a region of 20 channels of 1.27 km/s around the stellar velocity (+23.0 km/s, Torres et al. 2006). Secondly, a least-parameters approach was used, fitting a low-order polynomial only across the two green-shaded velocity ranges. The noise residual was 3.75 mK per channel in the latter case, and 4.00 mK in the former (this fit was possibly limited by the maximum 14th-order fit available in the SPLAT software). Subtracting the narrow-fit baseline results in a detection with 6.1 sigma confidence, and integrated line signal of 106.4 ± 17.5 mK km/s. The wide-fit baseline yields a 10.5 sigma detection of 200.0 ± 19.1 mK km/s. Both velocity-intervals were 14 channels wide. In the latter case, the remainder of the baselined spectrum could be used to check for false-positives, and the maximum integrated signal found in a sliding 14-channel-wide window was 17.1 mK km/s. The intensities are in a T_A^* antenna brightness temperature scale[2].

The preferred spectrum results from the wide-fit baseline subtraction, because the depth of the central minimum is more consistent with gas molecules on Keplerian orbits. Because of velocity projection effects, the central minimum should always have a positive signal, even for an infinitesimally-thin ring. The toy models shown adopt such a ring at 44 AU radius for the narrow-fit case, compared to a belt at 35-45 AU in the wide-fit case. The former model over-predicts the data by 2.4 sigma in the worst-case channel, and the latter by only 1.5 sigma. Also, the former case has a residual (summed variance between model and data) of 207 mK^2 compared to 164 mK^2 expected from random noise, while the latter fits within the noise (variance of 137 mK^2 compared to random expectation of 192 mK^2). The models are only intended to be indicative, but are informative as to possible locations of the gas orbits. For our fits to velocities in an edge-on disc around a 2.1 $M_\odot$ host star (Boccaletti et al. 2012), the radii thus point to molecules lying inwards of the dust – for example, Donaldson et al. (2013) have fitted a dust ring with a radius of around 110 AU.

There is a possible asymmetry between the red and blue sides of the line profile, which in the preferred fit have integrated intensities of 76.3 and 123.7 mK km/s respectively. The error on the difference is $\sqrt{2} \times 13.4$ mK km/s, so this has only 2.5 sigma confi-

[2] The Jy/K conversion factor for the JCMT is $15.6/\eta_a$, with aperture efficiency η_a having standard values of 0.52 and 0.61 at 345 and 230 GHz respectively.

Table 1. Literature data for the 27 debris-hosting A-stars within 125 pc that have been searched for CO, sub-divided into two age groups. The CII and OI lines were searched for with *Herschel*; the Herschel Science Archive was used to check a few unpublished spectra. Blank entries indicate no observation has been made, while u.l. denotes an upper limit. Stellar ages are from (1) Manoj et al. (2006); (2) TWA association: Ducourant et al. (2014); (3) LCC association: Song et al. (2012); (4) Rhee et al. (2007); (5) Beta Pic Moving Group: Mamajek & Bell (2014); (6) Kalas (2005); (7) Argus association: Zuckerman & Song (2012); (8) Tuc-Hor moving group: Bell et al. (2015); (9) Chen et al. (2014); (10) Mamajek (2012); (11) McDonald et al. (2012); (12) Monnier et al. (2012); (M) Moór et al. (2015,2006).

star	alias	spectral type	distance (pc)	age (Myr)	CO?	CII?	OI?	*incidences in age group*
HD141569		A0Ve	99	7 (1)	Yes	Yes	Yes	
HD109573	HR4796	A0	73	8 (2)	u.l.			
HD110058		A0V	107	10 (4)	u.l.			
HD131835		A2IV	123	16 (M)	Yes	u.l.	u.l.	
HD95086		A8III	90	17 (M)	u.l.			
HD121617		A1V	120	17 (M)	u.l.			
HD39060	betaPic	A6V	19	23 (5)	Yes	Yes	Yes	
HD172555		A7V	29	23 (5)	u.l.	u.l.	Yes	
HD181296	etaTel	A0V	48	23 (5)	u.l.	Yes	u.l.	
HD32297		A0V	112	30 (6)	Yes	Yes	u.l.	
HD38206		A0V	75	30 (M)	u.l.		u.l.	
HD85672		A0	93	30 (4)	u.l.			
HD9672	49Cet	A1V	59	40 (7)	Yes	Yes	u.l.	
HD3003	beta3Tuc	A0V	46	45 (8)	u.l.		u.l.	
HD21997	HR1082	A3IV/V	72	45 (8)	Yes	u.l.	u.l.	
HD102647	betaLeo	A3Va	11	50 (4)	u.l.			
								CO and/or C^+: 7/16 (44%); OI: 3/10 (30%)
HD110411		A0V	36	90 (M)	u.l.			
HD17848	nuHor	A2V	51	100 (4)	u.l.			
HD183324		A0V	61	140 (M)	u.l.			
HD182919		A0V	73	200 (M)	u.l.			
HD161868	gammaOph	A1V..	32	200 (4)	u.l.	u.l.		
HD95418		A1V	24	320 (9)	u.l.			
HD10939		A1V	62	350 (M)	u.l.			
HD216956	Fomalhaut	A4V	7.7	440 (10)	u.l.	u.l.	u.l.	
HD6028		A3V	91	500 (11)	u.l.			
HD158352	HR6507	A7V	60	600 (4)	u.l.	u.l.	u.l.	
HD172167	Vega	A0Va	7.7	700 (12)	u.l.	u.l.	u.l.	
								CO and/or C^+: 0/11 (0%); OI: 0/3 (0%)

dence. (In the narrow-fit case, the respective quantities are 33.4 and 73.0 mK km/s, differing at the 2.25 sigma level.)

A CO J=3-2 line towards HD 32297 is tentatively seen in a short JCMT observation with the HARP camera, from the archive. The integrated signal is 226 ± 92 mK km/s (2.5 sigma) over a v_{star} ± 9 km/s velocity range. However, Moór et al. (2011) reported a CO 3-2 upper limit from APEX which would translate to $\lesssim$150 mK km/s on the JCMT T_A^* scale, for nominal telescope efficiencies.

The mean intensities across the JCMT 2-1 and 3-2 lines are 11.3 ± 1.1 mK (wide-fit baseline case) and 12.7 ± 5.2 mK, with the latter value probably $\lesssim$8.4 mK for consistency with the APEX data. This gives a 3-2/2-1 line ratio of ~0.50 or less (after correction for the different beam-filling factors for a presumed point-like disc). In this case, the gas excitation temperature would be very low, at below ~5 K, but this only applies in a regime where both lines are taken to be optically thin. This is not true in some other systems, as noted below; see also Matrà et al. (2015) for further discussion of excitation of CO around an A-star.

3.3 CO census

From a master list of debris systems searched for CO rotational transitions, we find 27 A-star hosts within 125 pc of the Sun (Table 1). The most recent systematic survey is that of Moór et al. (2015), who also summarise previous work. The combined samples are close to complete for fractional dust luminosities $L_{dust}/L_* > 10^{-4}$, and have particularly targeted objects up to ages of 50 Myr. Our new target HD 32297 is the sixth system where a CO line has been detected. The earlier archetypes were found by Zuckerman et al. (1995), using the IRAM 30 m telescope to discover CO 2-1 emission around HD 145169 and 49 Ceti. Corresponding CO 3-2 lines were found with the JCMT (Dent et al. 1995, 2005). Moór et al. (2011, 2015) have subsequently discovered CO transitions in the HD 21997 and HD 131835 systems using the APEX 12m telescope. Dent et al. (2014) have been the first to map a distribution of CO, observing the 3-2 transition in the β Pic disc.

3.4 Properties of discs with gas

We now examine the seven C-hosting A-star systems, which have ages ranging from around 7 to 45 Myr (Table 1). This group is unified by the presence of CO and/or C^+ – and often both signatures, in support of the hypothesis that C^+ may be a by-product of CO photo-dissociation. (Observational limits may prevent this being universally seen: HD 21997 and HD 131835 have CO but only upper limits on CII, while η Tel shows CII but not CO.) In contrast,

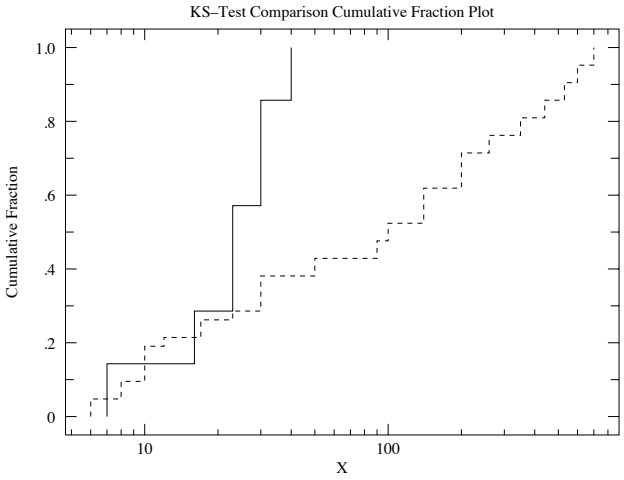

Figure 4. Cumulative distributions for debris discs with carbon gas (solid line) and without (dashed line), as functions of the stellar age in Myr.

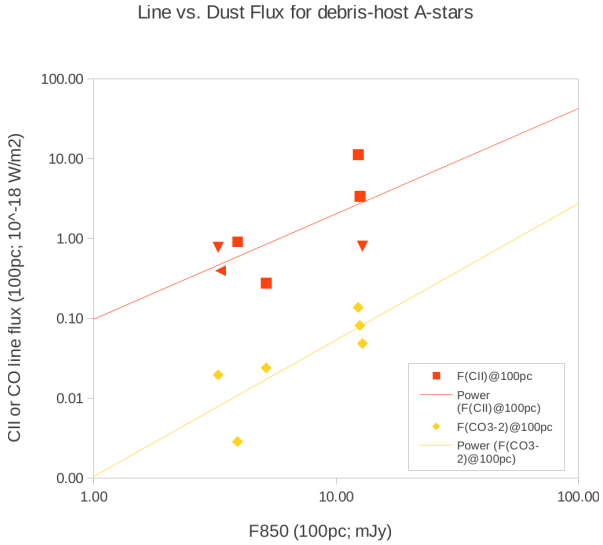

Figure 5. Correlations of gas and dust line fluxes (Table 2, but corrected to a common distance of 100 pc). Triangles represent upper limits; η Tel is omitted from the CO-correlation as it has limits on both axes (x ≤3.3, y ≤0.02).

OI persists for only about half as long, with the latest detection being in the 23 Myr Beta Pic Moving Group (BPMG). Strong OI emission is a characteristic of proto-planetary discs that are less evolved than debris discs (Dent et al. 2013).

Figure 4 shows cumulative distribution functions for the systems with and without carbon gas, as a function of the stellar age. At around 30 Myr, there is a divergence in the two populations, with carbon-bearing systems ceasing by 50 Myr, but two-thirds of the gas-less systems having greater ages. There do not seem to be strong selection effects, as the list of systems from Table 1 is spread quite evenly in log-age, reflecting a rather typical distribution for detectable solid debris. The age distribution is not intrinsically that of A-type stars, because debris fades with time (at a range of evolutionary rates). Further, CO searches have concentrated on systems with $L_{dust}/L_{*} > 10^{-4}$, which could introduce skews related to both evolution and detectability by distance – however, any biases here seem small. While less can be said about the older stars, the sampling of sub-50-Myr systems is very complete within our distance bound. Also, our median distance for stars ≤50 Myr old is 75 pc, similar to 60 pc for older stars and 70 pc for systems with CO/C+ detections. We conclude that carbon-bearing gas appears in nearly half of the well-studied group of debris systems around A-stars that are up to 50 Myr old – well beyond the sub-10 Myr epoch associated with gaseous proto-planetary discs.

The CO-hosting discs in Table 1 have dust luminosities characteristic of bright debris systems: L_{dust}/L_{star} values range from 5 10^{-4} to 7 10^{-3} (Table 2), within the 'luminous' classification of Moór et al. (2006). In contrast, proto-planetary discs are typified by $L_{dust}/L_{star} > 0.01$. This empirical boundary has recently been refined to criteria of $R_{12} < 3$ and $R_{70} < 2000$ (Wyatt et al. 2015), where R is the ratio of dust-to-photospheric emission and the wavelength-subscripts are in microns. By this definition, HD 141569 may be an intermediate case, with R_{12} of 6 (L_{dust}/L_{star} of 0.007), but still fairly distinct from gas-rich Herbig Ae stars. Hales et al. (2014) present a discussion of recent CO detections in HAe-type discs.

4 DISCUSSION

4.1 Correlations

Figure 5 plots the CO and CII fluxes versus the 850 micron dust emission. There are only 6-7 data points to examine for any trends, but it appears that both gases rise in brightness more steeply than the dust flux. For CO, the data can be fitted as F(CO) ∝ F(860μm)$^{1.7}$. This is suggestive of a trend where the mass in CO may scale with the production rate (i.e as the square of the dust mass), but a more detailed treatment of gas excitation and opacity is needed (see Moór et al. (2015), Figure 8, for the results of such analysis).

Here we have explored trends in CO flux versus disc mass, using the ProDiMo code (Woitke et al. 2016) to solve self-consistently for chemistry and radiative transfer in steady-state. The disc is assumed to have evolved into a 'late' proto-planetary stage, with a gas-to-dust mass ratio of 10, and dust that has settled downwards to a thin plane. While the disc chemistry produces CO emission that rises more steeply than disc mass (Figure 6), the absolute values of the line flux are too small compared to those observed. In particular, dust masses (Moór et al. 2015) of ≤1 $M_{\oplus}$ are at or below the left end of the x-axis, but CO J=3-2 line fluxes (Figure 5) lie at the top of the y-axis. This supports the hypothesis that these are *not* simply evolved proto-planetary discs, but that the CO molecules have a different origin. If their source is volatiles released from ices in collisions, then the starting point is not in fact an H-rich gas disc, and also the gas-phase chemistry will probably not be in steady state.

4.2 Asymmetries

Models predict that CO can have a very asymmetric spatial distribution, if the molecules originate from specific locations in the disc. This could occur in any model in which CO is produced by collisions between CO-ice bearing bodies and there are inhomogeneities in the density (and so collision rate) of the parent bodies. Examples of such models include points resonant with a planet, or

Table 2. Continuum and line fluxes for the A-stars with CO detections, plus the CII-detected system η Tel. The 850-870 micron fluxes are from observations here and in the literature, except for HD 32297 (estimated by interpolation over 500–1200 micron: Donaldson et al. 2013). The *Herschel*-detected lines of CII and OI are at wavelengths of 158 and 63 microns respectively. All line fluxes are in units of 10^{-18} W/m^2; continuum fluxes are in mJy (10^{-29} W/m^2/Hz). Uncertainties in brackets are 1-sigma and upper limits are 3-sigma.

	HD 141569	HD 131835	beta Pic	η Tel	HD 32297	49 Cet	HD 21997
L_{dust}/L_*	7e-3	3e-3	3e-3	2e-4	3e-3	1e-3	5e-4
F(850/870)	12.6(±4.6)	8.5(±4.4)	104(±10)	≤ 14.4	9(±3)	14.8(±3.1)	6.3(±1.6)
F(CO 3-2)	0.14(±0.1)	0.032(±0.006)	0.076(±0.008)	≤ 0.083	0.065(±0.027)	0.069(±0.014)	0.038(±0.006)
F(CO 2-1)	0.03(—)	≤0.018	≤ 0.03		0.037(±0.004)	0.013(—)	0.018(±0.004)
F(CII)	11.4(±1.8)	≤0.5	24.3(±0.4)	1.7(±0.4)	2.68(±0.72)	0.80(±0.17)	≲ 1.5
F(OI)	245(±5)	≤1.5	≈ 7		≤ 7.3	≤ 11	≲ 2.7

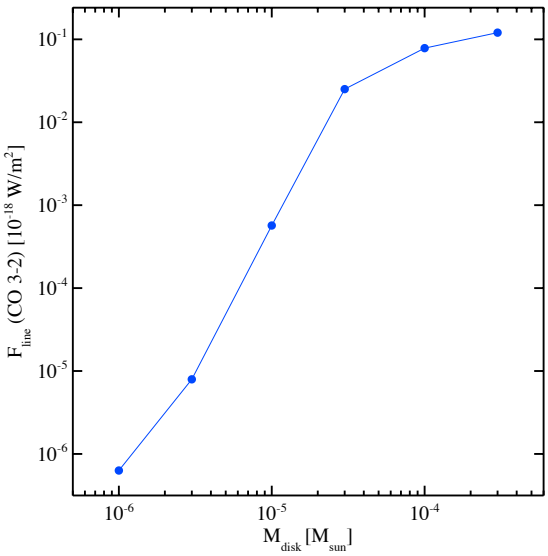

Figure 6. ProDiMo code results. The host star is at 100 pc with T_{eff} = 8600 K, L_* = 14 $L_\odot$, X-ray flux of 10^{29} erg and UV flux of 0.1 L_*. The power-law distribution of dust sizes has a -3.5 index over 0.01 to 300 mm. The gas mass is ten times that of dust, and abundances are solar. The debris spans 30-100 AU in radius, with vertical height H(r) $\propto r^1$, to 10 AU height at 100 AU radius. The dust is settled to a thin mid-plane layer. The column density through the disc scales as $\Sigma(r) \propto r^{-1}$, with exponential tapering inward of 40 AU and outward of 50 AU.

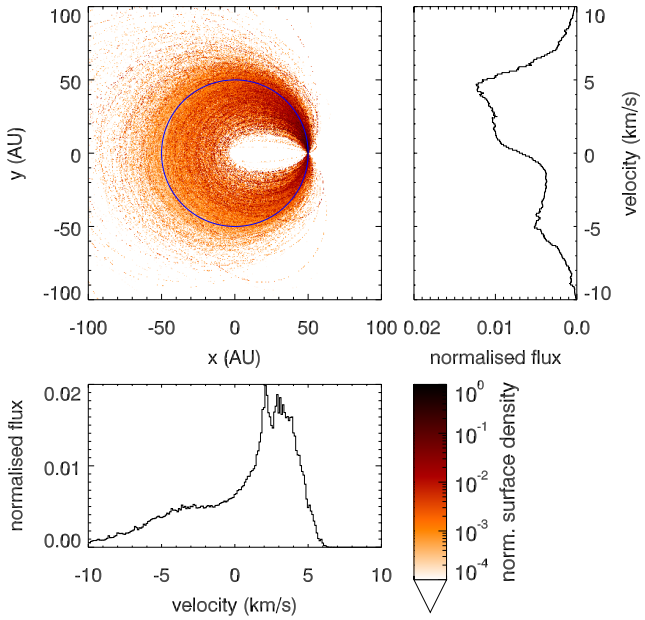

Figure 7. Example of CO production for a giant impact model. The top-left panel shows the spatial distribution of CO in a face-one view of the disk. The bottom and top-right panels show spectra for the CO as viewed edge-on from the bottom and right of the image respectively. The impact of an anti-clockwise-orbiting progenitor occurs at 50 AU from a 1.5 solar-mass star, producing a velocity dispersion of 0.3 times the circular Keplerian speed (see Jackson et al. 2014). The CO decays exponentially with a timescale of 120 years after production.

the site of the break-up of a massive planetesimal. The asymmetry in the debris is enhanced for CO because of its short photodissociation timescale, so that the molecules are most concentrated at their point of origin. Jackson et al. (2014) have modelled this scenario for the case of a giant impact/break-up event, and Figure 7 illustrates how the observational outcome can vary for different viewing directions. The spectra are strongly asymmetric, but the shape of the spectrum varies considerably with the (generally unknown) viewing angle, complicating the interpretation. An additional complication is that the simple model in Figure 7 only includes the Keplerian orbital motion of the CO gas, and does not include the effect of gas pressure, which may be significant at higher CO densities. This would change the shape of the lines in Figure 7, but would not remove the large scale asymmetry in the line profiles.

In Figure 8, whole-disc CO line-profiles are shown for four systems. For β Pic, archival ALMA observations in CO J=2-1 were used to generate disc-integrated spectra (with sensitivity up to arcmin scales). For 49 Ceti and HD 141569, we used CO 3-2 lines extracted from single-beam JCMT data[3]. The plots show tests for asymmetry, where the line velocities around the central dip have been swapped in sign, and used to generate a blue-red difference spectrum. Where this residual is non-zero, the emission from the the approach and receding sides of the disc is not the same, as for example in many sightlines across the model disc in Figure 7.

[3] For HD 141569, data from 2009 were used, with earlier archival spectra from 1995 and 2001 showing similar profiles.

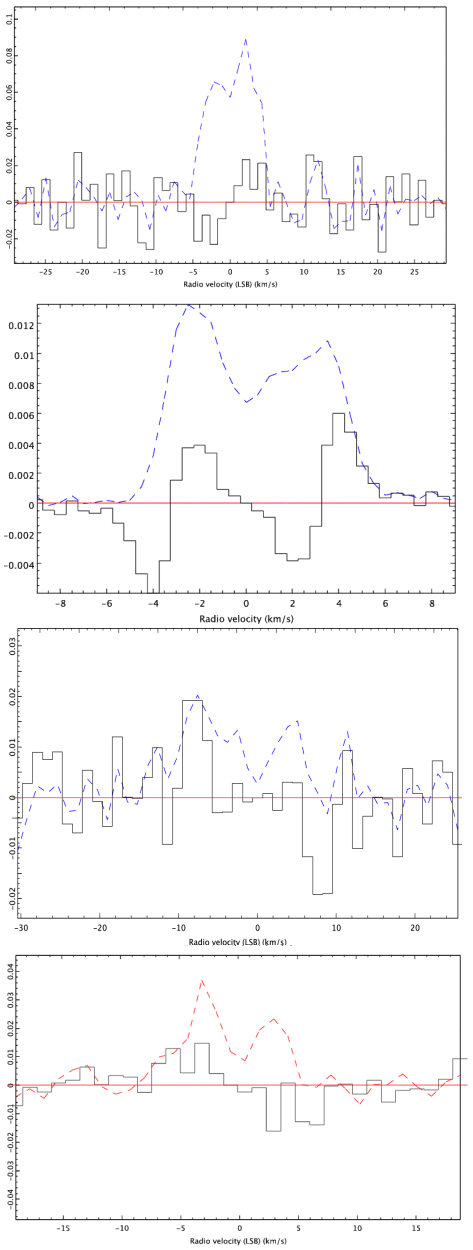

Figure 8. CO whole-disc line profiles, and blue-red difference spectra (see text). From top to bottom: HD 141569 observed in CO 3-2; β Pic in CO 2-1; HD 32297 in CO 2-1 (this work); 49 Cet in CO 3-2. Spectra of HD 21997 and HD 131835 (from APEX: Moór et al. 2011, 2015) are symmetric within the noise, and are omitted. Y-axis units (not shown) are native to each dataset; actual (dashed) and difference spectra are on the same scale within each plot. X-axis units are velocity with respect to the line-centre minimum-signal point.

From this analysis, we find that CO asymmetry is most marked in β Pic. The high signal-to-noise line is asymmetric in both height and width of the blue and red sides, reflecting the clump that has been spatially resolved (Dent et al. 2013). For 49 Ceti, the overall line shape appears similar to β Pic, but the nature of any asymmetry is hard to characterise. Hughes (2014) has presented ALMA observations of the 49 Ceti disc (sampling scales only up to $\approx$10 arcsec) and the line profile shows some differences to that from the JCMT. Extended emission could thus be affecting the single dish spectrum, although it appears uncontaminated by the northern object seen by SCUBA-2 (ALMA sees no low-velocity CO here). The line asymmetry for HD 32297 is only at 2.5-sigma confidence, and the visual appearance of asymmetry for HD 141569 is at the level of noise in the difference spectrum.

Table 3. Asymmetry measures for gas and dust. For CO, the ratio given is of integrated intensity over two half-lines, with the mid-point defined as the faintest line-centre channel. For dust images, the ratio given is of integrated flux on either side of the star along the major axis; for the single dish data these estimates only compare two beams. Data include: HD 141569 – CO 3-2 (JCMT), 0.87 mm dust (LABOCA); HD131835 – CO 3-2 (APEX), 0.87 mm (LABOCA); β Pic – CO 2-1 and 0.87 mm dust (ALMA); HD 21997 – CO 2-1, 3-2 (APEX), 0.85 mm dust (JCMT); HD 32297 – CO 2-1 (JCMT), 1.3 mm dust (CARMA); 49 Cet – CO 3-2 (JCMT, ALMA), 0.87 dust (ALMA). LABOCA images are from Nilsson et al. (2010); other references are given above.

star	CO line asymmetry	mm dust asymmetry	notes
HD 141569	1.0±0.2	$\gtrsim$1.5	opt. thick CO
HD 131835	~1.3	~1.3	opt. thick CO?
β Pic	$\approx$2	$\approx$1.2	CO more asym.
HD 32297	1.6±0.3	$\approx$2	similar asym.
49 Cet	~1.8	$\approx$1.1	CO more asym?
HD 21997	$\approx$1.0	$\approx$2.3	opt. thick CO

Owing to the short dissociation time for CO molecules, whole-disc spectra might be expected to be more skewed than the dust distributions. Table 3 attempts to quantify this using the integrated intensities of the blue/red sides of the CO lines, and the total dust fluxes observed to either side of the star. The available data are rather eclectic, but two systems do hint at the expected skewness behaviour. Both β Pic and 49 Cet appear more asymmetric in CO than in dust, using these measures, although the CO profile for the latter is uncertain, as discussed above. HD 32297 and HD 131835 have spectral data too noisy to discriminate, while HD 21997 and HD 141569 appear more asymmetric in *dust*. However, these two systems appear to have optically thick CO lines such that saturation would maximise intensity in both line-halves. The less abundant isotopologue ^{13}CO has recently been imaged in the 2-1 transition (HD 21997: Kospál et al. 2013; HD 141569: Péricaud et al. 2016), and greater blue/red asymmetry begins to appear in these less saturated lines. Both of these studies found large masses of CO, however, that may be inconsistent with sources in a comet belt. The implications for the origin of the gas (collisional versus remnant proto-planetary discs) are discussed by Zuckerman & Song (2012) and Moór et al. (2015).

5 CONCLUSIONS

With the discovery of CO molecules around HD 32297, there are now six A-type main-sequence stars where dusty debris is known to be accompanied by carbon monoxide gas. In the age bracket spanning 5-50 Myr, nearly half of the A-stars with debris in fact exhibit carbon-bearing gas. This suggests a prolonged active epoch where giant collisions release a burst of gas from frozen volatiles. The time period is similar to that taken to assemble the Earth from colliding planetesimals (e.g. Jacobson & Walsh 2015), so further study may yield clues to how volatiles are folded into rocky planets and their atmospheres.

As the photo-dissociation time for CO around A-type stars is short, the gas profiles will tend to be asymmetric if debris origi-

nates from one spatial location, with molecules mainly on one side of the star. This is supported for 1-2 systems where the gas asymmetry appears to exceed that of the dust. Models can explain a high incidence of CO detection when the molecules are short-lived if, for example, colliding debris repeatedly passes through the original impact point. However, at least two of the discs are optically thick in CO emission, suggesting the gas may not be collisional, but instead represent a very prolonged proto-planetary disc phase.

ACKNOWLEDGMENTS

Data were obtained under JCMT project IDs MJLSD01 and M13BU16. JSG and PW thank the ERC for funding for project DiscAnalysis, under the grant FP7-SPACE-2011 collaborative project 284405. JPM is supported by a UNSW Vice-Chancellor's postdoctoral fellowship. MCW and LM acknowledge the support of the European Union through ERC grant 279973.

The James Clerk Maxwell Telescope is operated by the East Asian Observatory on behalf of The National Astronomical Observatory of Japan, Academia Sinica Institute of Astronomy and Astrophysics, the Korea Astronomy and Space Science Institute, the National Astronomical Observatories of China and the Chinese Academy of Sciences (Grant No. XDB09000000), with additional funding support from the Science and Technology Facilities Council of the United Kingdom and participating universities in the United Kingdom and Canada. ALMA is a partnership of ESO (representing its member states), NSF (USA) and NINS (Japan), together with NRC (Canada), NSC and ASIAA (Taiwan), and KASI (Republic of Korea), in cooperation with the Republic of Chile. The Joint ALMA Observatory is operated by ESO, AUI/NRAO and NAOJ.

References

Bell C.P.M., Mamajek E.E., Naylor M., 2015, MNRAS 454, 593
Boccaletti A. et al., 2012, A& 544, A85
Chen C.H. et al., 2014, ApJS 211, 25
Dent W.R.F. et al., 2014, Science 343, 1490
Dent W.R.F. et al., 2013, PASP 125, 477
Dent W.R.F., Greaves J.S., Coulson I M., 2005, MNRAS 359, 663
Dent W.R.F., Greaves J.S., Mannings V., Coulson I.M., Walther D.M., 1995, MNRAS 277, L25
Donaldson J.K., Lebreton J., Roberge A., Augereau J.-C., Krivov A.V., 2013, ApJ 772, 17
Ducourant C. et al., 2014, A&A 563, id.A121
Hales A.S., 2014, AJ 148, 47
Holland W.S. et al., 2013, MNRAS 430, 251
Hughes A.M., 2014, conference presentation archived at http://www.ast.cam.ac.uk/talks/archive/3445
Hughes A.M., Wilner D.J., Kamp I., Hogerheijde M.R., 2008, ApJ 681 626
Jackson A.P.., Wyatt M.C., Bonsor A., Veras D., 2014, MNRAS 440, 3757
Jenness T., Berry D., Chapin E., Economou F., Gibb A., Scott D., 2011, ASPC 442, 281
Kalas P., 2005, ApJ 635, L169
Kóspál Á. et al., 2013, ApJ 776, 77
Kral Q., Wyatt M. C., Carswell R. F., Pringle J. E., Matrà L., Juhász Á., 2016, MNRAS, submitted
Lieman-Sifry J., Hughes A.M., 2015, AAS #225, id.349.18
Mamajek E.E., Bell C.P.M., 2014, MNRAS 445, 2169
Mamajek E.E., 2012, ApJ 754, L20
Maness H.L., Fitzgerald M.P., Paladini R., Kalas P., Duchene G., Graham J.R., 2008, ApJ 686, L25
Manoj P., Bhatt H.C., Maheswar G., Muneer S., 2006, ApJ 653, 657
Matrà L., Panić O., Wyatt M.C., Dent W.R.F., 2015 MNRAS 447 3936
McDonald I., Zijlstra A.A., Boyer M.L., 2012, MNRAS 427, 343
Monnier J.D et al., 2012, ApJ 761, L3
Montgomery S.L., Welsh B.Y., PASP 124, 1042
Moór A. et al., 2015, MNRAS 447, 577
Moór A. et al., 2013, ApJ 777, L25
Moór A. et al., 2011, ApJ 740, L7
Moór A. et al., 2006, ApJ 644, 525
Nilsson R., 2010, A&A 518, 40
Panić O. et al., 2013, MNRAS 435, 1037
Panić O., van Dishoeck E.F., Hogerheijde M.R., Belloche A., Güsten R., Boland W., Baryshev A., 2010, A&A 519, 110
Péricaud J., di Folco E., Dutrey A., Augereau J.-C., Piétu V., Guilloteau S., 2016, IAUS 314, 201
Redfield S, 2007, ApJ 656 L97
Rhee J.H., Song I., Zuckerman B., McElwain M., 2007, ApJ 650, 1556 Rieke G.H. et al., 2005, ApJ 620, 1010
Roberge A. et al., 2013, ApJ 771, 69
Song I., Zuckerman B., Bessell M.S., 2012, AJ 144, id.8
Torres C.A.O., Quast G.R., Da Silva L., De La Reza R., Melo C.H.F., Sterzik M., 2006, A&A 460, 695
Woitke P. et al., 2016, A&A 586, 103
Wyatt M.C., Panić O., Kennedy G.M., Matrà L., 2015, Ap&SS 357, 103
Zuckerman B., Song I., 2012, ApJ 758 77
Zuckerman B., Forveille T., Kastner J.H., 1995, Nature 373, 494

This paper has been typeset from a TEX/ LATEX file prepared by the author.